

In-motion initial alignment method for a laser Doppler velocimeter-aided strapdown inertial navigation system based on an adaptive unscented quaternion H-infinite filter

Zhiyi Xiang, Qi Wang, Rong Huang, Chongbin Xi, Xiaoming Nie and Jian Zhou* 

College of Advanced Interdisciplinary Studies, National University of Defense Technology, Changsha 410073, People's Republic of China

E-mail: wttzhoujian@163.com

Received 16 June 2021, revised 10 September 2021

Accepted for publication 9 November 2021

Published 22 December 2021



CrossMark

Abstract

With its advantages of high velocity measurement accuracy and fast dynamic response, the laser Doppler velocimeter (LDVs) is expected to replace the odometer (OD) in combination with a strapdown inertial navigation system (SINS) to give a higher-precision integrated navigation system. Since a LDV has higher velocity measurement accuracy and data update frequency than an OD and Doppler velocity log, a LDV is used for the first time in this paper to aid a SINS in in-motion alignment. Considering that some approximation is used in the alignment model, the uncertainty noise of the sensors during the motion process and the unknown noise parameters during the filter process, an adaptive unscented quaternion H-infinite estimator (AUSQUHE) is proposed. The proposed AUSQUHE method has high robustness since it combines the advantages of an unscented quaternion estimator and H-infinite filter. The adaptive threshold of the H-infinite filter and the adaptive measurement noise covariance matrix are introduced to make the filter adapt to the changing environment and accelerate the convergence of errors. The performance of the proposed method is verified by a vehicle field test with a normal LDV signal and a vehicle test with the LDV signal disturbed by noise. The results show that the proposed method has higher alignment accuracy, faster convergence speed and stronger robustness than the four other compared methods.

Keywords: laser Doppler velocimeter (LDV), strapdown inertial navigation system (SINS), in-motion alignment, adaptive unscented quaternion H-infinite estimator (AUSQUHE)

(Some figures may appear in color only in the online journal)

* Author to whom any correspondence should be addressed.

1. Introduction

Strapdown inertial navigation systems (SINSs) have been widely used in aerospace, military, industrial and consumer fields because of their self-containment, anti-jamming capability, high sampling rate and good concealment [1]. In recent years, the application of SINSs in vehicles has attracted increasing attention. The initial alignment determines the attitude matrix between the body frame and the navigation frame since the inertial measurement unit (IMU) provides the angular rate and acceleration in the body frame whereas the purpose of navigation is to determine the position of the vehicle in the navigation frame [2, 3]. The initial alignment of the SINS is one of the key technologies that affect the accuracy of vehicle navigation, and the accuracy and speed of the initial alignment directly affect the accuracy of the SINS [4], so the initial alignment of a SINS has been a hot research topic.

Motivated by many military applications and commercial aviation, many researchers have studied and achieved excellent results in in-motion alignment [5]. Because acceleration of a vehicle relative to the ground occurs during vehicle movement, it is difficult to obtain accurate gravity information for the vehicle in the inertial frame. As a result, it is impossible to complete an accurate in-motion initial alignment process relying only on the measurement of the gyroscope and accelerometer of the SINS. To solve this problem, the external velocity measuring device is used to help the SINS to complete the in-motion alignment, and many effective methods have been developed. For a high-accuracy SINS, an optimization-based alignment (OBA) method using global positioning system (GPS) velocity was proposed [6]. In the OBA method the attitude matrix is decomposed into two time-varying attitude matrices and a constant attitude matrix. The two time-varying attitude matrices are calculated by the body angular rate and the navigation angular rate, respectively, and the constant attitude matrix is obtained by Davenport's q-method based on the constructed vector observations [7]. Since then, researchers have continuously improved the OBA method and expanded the scope of its application, such as the GPS velocity-based OBA method [8], the odometer (OD) velocity-based OBA method [9], the Doppler velocity log (DVL) velocity-based OBA method [10], the GPS position loci-based OBA method [11], the sliding-window-based OBA method and so on [12]. By combining the OBA method with a Kalman filter, the defect of the traditional OBA method (that it cannot estimate the IMU bias) was solved, and the accuracy of the OBA method improved [13–15]. To complete in-motion initial alignment of a low-cost SINS, an alignment method combining the OBA method and an unscented quaternion estimator (USQUE) was proposed, in which the USQUE was used to jointly estimate the gyroscope bias and attitude errors [16, 17]. In addition, the USQUE was used separately for in-motion alignment because it can estimate attitude error as well as other error parameters and handle the noise in the model [18]. As a variant of the unscented Kalman filter (UKF), USQUE lacks adaptive ability to system noise and converges slowly at large

unknown initial attitude errors. In recent years, many useful methods of in-motion alignment have been proposed, but they all used GPS, OD or DVL as velocity sensors and seldom considered the influence of non-Gaussian noises such as outliers during the operation of these sensors in in-motion alignment.

Based on the laser Doppler effect, a laser Doppler velocimeter (LDV) has the advantages of high accuracy, rapid dynamic response, non-contact measurement, good directional sensitivity, complete autonomy and good spatial resolution, and thus LDVs have been extensively used in biomedicine, meteorological observation, fluid flow velocity measurement and so on [19, 20]. In recent years, our research group has proposed and developed a variety of LDVs with a reference-beam structure to measure the true vehicle velocity over ground and which have a higher velocity measurement accuracy than OD and DVL methods [21–23]. In this paper, LDV is used for the first time to aid SINS in in-motion alignment and a new fast robust in-motion alignment method, named the adaptive unscented quaternion H-infinite estimator (AUSQUHE), is proposed to improve the alignment accuracy and speed.

The features and advantages of proposed the in-motion alignment method are as follows:

- (a) LDV is used for the first time to aid SINS to complete in-motion alignment, which will expand the application range of LDV, and the high-precision velocity provided by LDV is expected to shorten the time needed for SINS in-motion alignment.
- (b) It represents a new attempt to fuse USQUE with an H-infinite filter and use it for in-motion alignment. It avoids possible singularity problems and quaternion normative constraint problems in order to complete alignment at large misalignment angles, and reduces the influence of inaccurate parameter setting, model approximation and uncertain noise on the alignment result.
- (c) The adaptive threshold of the H-infinite filter is proposed to make the in-motion alignment process more adaptable to changes in the environment.
- (d) Adaptive processing of the noise covariance matrix helps the filter to maintain good performance without divergence. Meanwhile, the noise covariance matrix with smaller error accelerates the convergence of attitude error.
- (e) The proposed in-motion alignment method does not increase the time complexity significantly, and it is suitable for real-time alignment.

The rest of this paper is organized as follows. In section 2, the vector observations of the in-motion alignment for LDV/SINS integration are deduced mathematically, and the process model and observation model are established. In section 3, the AUSQUHE is proposed. In section 4, the proposed method is compared with the existing typical methods using vehicle-mounted field test data collected from a LDV-aided laser SINS. Concluding remarks are given in section 5.

2. In-motion alignment for LDV/SINS

In this paper, the local level navigation frame is denoted as the n frame, the vehicle body frame is denoted as the b frame, the inertial non-rotating frame is denoted as the i frame and the earth frame is denoted as the e frame.

The velocity kinematic equation in the n frame is given by

$$\dot{\mathbf{v}}^n = \mathbf{C}_{b(t)}^n \mathbf{f}^b - (2\boldsymbol{\omega}_{ie}^n + \boldsymbol{\omega}_{en}^n) \times \mathbf{v}^n + \mathbf{g}^n \quad (1)$$

where $\mathbf{v}^n = [v_E^n \ v_N^n \ v_U^n]^T$ is the ground velocity in the n frame, \mathbf{f}^b is the specific force in the b frame, \mathbf{g}^n is the gravity vector in the n frame, $(\cdot) \times$ means to solve the antisymmetric matrix, $\boldsymbol{\omega}_{ie}^n$ is the earth rotation rate with respect to the i frame and $\boldsymbol{\omega}_{en}^n$ is the navigational rotating rate in the n frame relative to the e frame. $\boldsymbol{\omega}_{ie}^n$ and $\boldsymbol{\omega}_{en}^n$ can be expressed, respectively, as

$$\boldsymbol{\omega}_{ie}^n = [0, \omega_{ie} \cos L, \omega_{ie} \sin L]^T \quad (2)$$

$$\boldsymbol{\omega}_{en}^n = \left[-\frac{v_N^n}{R_M + h}, \frac{v_E^n}{R_N + h}, \frac{v_U^n}{R_N + h} \tan L \right]^T \quad (3)$$

where ω_{ie} is the earth's rotation speed, L is the local latitude, h is the local altitude and R_M and R_N are the principal radius of curvature of the prime meridian and the equator, respectively.

According to the coordinate transformation method

$$\dot{\mathbf{v}}^n = (\mathbf{C}_b^n \mathbf{v}^b)' = \mathbf{C}_b^n (\dot{\mathbf{v}}^b + \boldsymbol{\omega}_{nb}^b \times \mathbf{v}^b) \quad (4)$$

where $\boldsymbol{\omega}_{nb}^b$ is body angular rate with respect to the n frame.

Substituting equation (4) into equation (1) yields

$$\mathbf{C}_b^n (\dot{\mathbf{v}}^b + (\boldsymbol{\omega}_{ib}^b + \boldsymbol{\omega}_{ie}^b) \times \mathbf{v}^b - \mathbf{f}^b) = \mathbf{g}^n. \quad (5)$$

2.1. Process model

According to the chain rule of the direction cosine matrix, the attitude matrix $\mathbf{C}_b^n(t)$ can be expressed as

$$\mathbf{C}_b^n(t) = \mathbf{C}_{n(0)}^n(t) \mathbf{C}_{b(0)}^{n(0)} \mathbf{C}_{b(t)}^{b(0)} \quad (6)$$

where $b(0)$ and $n(0)$ denote the initial b frame and n frame, respectively, which are both non-rotating orthogonal frames with respect to the i frame.

Assuming that the velocity provided by the LDV is accurate, it is necessary to incorporate it into the process model and measurement model. In order to achieve this, we denote the initial b frame as an inertial frame. Equation (6) and the attitude update equation can be written as

$$\mathbf{C}_b^n(t) = \mathbf{C}_i^n(t) \mathbf{C}_{b(t)}^i \quad (7)$$

$$\dot{\mathbf{C}}_{b(t)}^i = \mathbf{C}_{b(t)}^i (\boldsymbol{\omega}_{ib}^b \times) \quad (8)$$

$$\dot{\mathbf{C}}_{n(t)}^i = \mathbf{C}_{n(t)}^i (\boldsymbol{\omega}_{in}^n \times) \quad (9)$$

where

$$\boldsymbol{\omega}_{in}^n = \boldsymbol{\omega}_{ie}^n + \boldsymbol{\omega}_{en}^n. \quad (10)$$

Equation (9) is the process model of the proposed method.

2.2. Measurement model

Substituting equation (7) into equation (5) and multiplying by $\mathbf{C}_{n(t)}^i$ on both sides we get

$$\mathbf{C}_{b(t)}^i (\dot{\mathbf{v}}^b + (\boldsymbol{\omega}_{ie}^b + \boldsymbol{\omega}_{ib}^b) \times \mathbf{v}^b - \mathbf{f}^b) = \mathbf{C}_{n(t)}^i \mathbf{g}^n. \quad (11)$$

Integrating the time interval of interest on both sides of equation (11), it can be obtained that

$$\begin{aligned} \mathbf{C}_{b(t)}^i \mathbf{v}^b(t) - \mathbf{v}^b(0) + \int_0^t \mathbf{C}_{b(\tau)}^i (\boldsymbol{\omega}_{ie}^b \times \mathbf{v}^b) d\tau - \int_0^t \mathbf{C}_{b(\tau)}^i \mathbf{f}^b d\tau \\ = \mathbf{C}_{n(t)}^i \mathbf{C}_{n(0)}^{n(t)} \int_0^t \mathbf{C}_{n(\tau)}^{n(0)} \mathbf{g}^n d\tau. \end{aligned} \quad (12)$$

We define the two vectors as

$$\begin{cases} \boldsymbol{\alpha}(t) = \mathbf{C}_{b(t)}^i \mathbf{v}^b(t) - \mathbf{v}^b(0) + \int_0^t \mathbf{C}_{b(\tau)}^i (\boldsymbol{\omega}_{ie}^b \times \mathbf{v}^b) d\tau \\ \quad - \int_0^t \mathbf{C}_{b(\tau)}^i \mathbf{f}^b d\tau \\ \boldsymbol{\beta}(t) = \mathbf{C}_{n(t)}^i \int_0^t \mathbf{C}_{n(\tau)}^{n(0)} \mathbf{g}^n d\tau \end{cases}. \quad (13)$$

The measurement model can be given by

$$\boldsymbol{\alpha}(t) = \mathbf{C}_{n(t)}^i \boldsymbol{\beta}(t). \quad (14)$$

In order to facilitate the process on computer, it is necessary to discretize equation (13). The first integral in equation (13) can be calculated as

$$\begin{aligned} \int_0^t \mathbf{C}_{b(\tau)}^i (\boldsymbol{\omega}_{ie}^b \times \mathbf{v}^b) d\tau \\ = \sum_{k=0}^{M-1} \mathbf{C}_{b(t_k)}^i \mathbf{C}_{n(t_k)}^{b(t_k)} \int_{t_k}^{t_{k+1}} \mathbf{C}_{n(\tau)}^{n(t_k)} (\boldsymbol{\omega}_{ie}^n \times) \mathbf{v}^n(\tau) d\tau. \end{aligned} \quad (15)$$

According to [7], the incremental integral in equation (15) can be approximated by

$$\begin{aligned} \Delta \mathbf{v}^n(t_k) &= \int_{t_k}^{t_{k+1}} \mathbf{C}_{n(\tau)}^{n(t_k)} (\boldsymbol{\omega}_{ie}^n \times) \mathbf{v}^n(\tau) d\tau \\ &= \left(\frac{T}{2} \mathbf{I}_3 + \frac{T^2}{6} \boldsymbol{\omega}_{in}^n \times \right) \boldsymbol{\omega}_{ie}^n \times \mathbf{v}^n(t_k) \\ &\quad + \left(\frac{T}{2} \mathbf{I}_3 + \frac{T^2}{3} \boldsymbol{\omega}_{in}^n \times \right) \boldsymbol{\omega}_{ie}^n \times \mathbf{v}^n(t_{k+1}). \end{aligned} \quad (16)$$

The second integral in equation (13) can be calculated as

$$\int_0^t \mathbf{C}_{b(\tau)}^i \mathbf{f}^b d\tau = \sum_{k=0}^{M-1} \mathbf{C}_{b(t_k)}^i \int_{t_k}^{t_{k+1}} \mathbf{C}_{b(\tau)}^{b(t_k)} \mathbf{f}^b(\tau) d\tau. \quad (17)$$

According to [7], two-sample correction is used to approximate the incremental integral in equation (17)

$$\begin{aligned} \Delta \mathbf{v}^{b(t_k)} &= \int_{t_k}^{t_{k+1}} \mathbf{C}_{b(\tau)}^{b(t_k)} \mathbf{f}^b(\tau) d\tau \\ &= \Delta \mathbf{v}_1 + \Delta \mathbf{v}_2 + \frac{1}{2} (\Delta \theta_1 + \Delta \theta_2) \times (\Delta \mathbf{v}_1 + \Delta \mathbf{v}_2) \\ &\quad + \frac{2}{3} (\Delta \theta_1 \times \Delta \mathbf{v}_2 + \Delta \mathbf{v}_1 \times \Delta \theta_2). \end{aligned} \quad (18)$$

According to the aforementioned derivation, the discrete form of equation (13) can be expressed as

$$\begin{cases} \alpha(t) = \mathbf{C}_{b(t_M)}^i \mathbf{v}^b(t_M) - \mathbf{v}^b(0) \\ \quad + \sum_{k=0}^{M-1} \mathbf{C}_{b(t_k)}^i \mathbf{C}_{n(t_k)}^{b(t_k)} \Delta \mathbf{v}^{n(t_k)} - \sum_{k=0}^{M-1} \mathbf{C}_{b(t_k)}^i \Delta \mathbf{v}^{b(t_k)} \\ \beta(t) = \mathbf{C}_{n(t_M)}^{n(0)} \sum_{k=0}^{M-1} \mathbf{C}_{n(t_k)}^{n(0)} \left(\mathbf{I} \mathbf{I}_3 + \frac{T^2}{2} \boldsymbol{\omega}_{in}^n \times \right) \mathbf{g}^n(t_k) \end{cases} \quad (19)$$

where T is the sampling interval.

3. Proposed AUSQUHE algorithm

The mainstream OBA method requires the constructed model to have high precision, so most OBA methods are developed for GPS-aided SINS. Compared with GPS, LDV cannot provide accurate position and velocity information directly, and may degrade the alignment performance of the OBA method. USQUE is a method based on attitude estimation; besides attitude estimation, it can also estimate other parameters, which is not feasible in OBA method. However, as a quaternion application form of the UKF, USQUE lacks the self-adaptive capacity to deal with system noise, and has poor alignment accuracy and slow convergence speed when the noise characteristics are uncertain. Hence AUSQUHE is proposed to solve this problem. Equations (9) and (14) formulate the continuous process and measurement model.

The direct implementation of a UKF with a quaternion-based state is not suitable because the quaternion estimate is determined using the weighted quaternion averaging operation. Thus, no guarantee can be made that the quaternion will have unit norm. To represent an attitude-error quaternion preserving the constraint of quaternion propagation, the quaternion is used for attitude propagation and the unconstrained three-component vectors of generalized Rodrigues parameters (GRP) are used for filtering and local attitude error representation.

Denote the error of the attitude error quaternion by $\delta \mathbf{q} = [\delta q_0, \delta \mathbf{q}_{1:3}^T]^T = [\delta q_0, \delta \boldsymbol{\rho}^T]^T$, the corresponding GRP representation $\delta \mathfrak{R}$ is given by

$$\delta \mathfrak{R} = f \frac{\delta \boldsymbol{\rho}}{a + \delta q_0} \quad (20)$$

where a is a parameter from 0 to 1 and f is a scale factor. The GRP is used to place the singularity of the attitude representation in a certain angle range, and different combinations of a and f have different physical meanings. For example,

when $a = 0$ and $f = 1$, equation (20) gives the Gibbs vector, and when $a = f = 1$, equation (20) gives the standard vector of modified Rodrigues parameters.

The inverse transformation from $\delta \mathfrak{R}$ to $\delta \mathbf{q}$ is given by

$$\begin{cases} \delta q_0 = \frac{-a \|\delta \mathfrak{R}\|^2 + f \sqrt{f^2 + (1-a)^2 \|\delta \mathfrak{R}\|^2}}{f^2 + \|\delta \mathfrak{R}\|^2} \\ \delta \boldsymbol{\rho} = f^{-1} (a + \delta q_0) \delta \mathfrak{R} \end{cases} \quad (21)$$

In AUSQUHE, the filtering state is defined as

$$\hat{\mathbf{X}}_k = [\delta \mathfrak{R}_k^T \quad \hat{\mathbf{X}}_k^{eT}]^T \quad (22)$$

where $\hat{\mathbf{X}}_k^e$ is the components of the state besides the quaternion. In this paper, considering the high-precision SINS and LDV adopted and the short alignment time, other parameters are not estimated to reduce the amount of calculation.

We write the measurement model (14) as follows:

$$\mathbf{y}_k = \boldsymbol{\alpha}(k) - \mathbf{C}_{n(k)}^i \boldsymbol{\beta}(k) = \mathbf{h}(\mathbf{X}_k) + \mathbf{v}_k \quad (23)$$

where \mathbf{X}_k is the ideal value of the filtering state at time instant k and \mathbf{v}_k is the measurement noise.

The state estimation at time instant k is $\hat{\mathbf{X}}_k$, the corresponding covariance is $\mathbf{P}_{x,k}$, and the AUSQUHE algorithm for initial alignment is described as follows.

3.1. Time update

Generate the sigma points as

$$\chi_k(i) = \begin{cases} \hat{\mathbf{X}}_k, i = 0 \\ \hat{\mathbf{X}}_k + \left[\sqrt{(n+\lambda) \mathbf{P}_{x,k}} \right]_i, i = 1, 2, \dots, n \\ \hat{\mathbf{X}}_k - \left[\sqrt{(n+\lambda) \mathbf{P}_{x,k}} \right]_i, i = n+1, n+2, \dots, 2n \end{cases} \quad (24)$$

where n is the dimension of $\hat{\mathbf{X}}_k$, $\lambda = \sigma^2 (n + \kappa) - n$, σ is scale factor with a typical value range of $10^{-4} \leq \sigma \leq 1$ and κ is tune parameter, which is usually set to 0 and $3n$ to capture some higher-order information about the distribution.

The weighted weights of the expectation and covariance matrices can be calculated, respectively, as

$$\mathbf{W}^m(i) = \begin{cases} \frac{\lambda}{n+\lambda}, i = 0 \\ \frac{1}{2(n+\lambda)}, i = 1, \dots, 2n \end{cases} \quad (25)$$

$$\mathbf{W}^c(i) = \begin{cases} \frac{\lambda}{n+\lambda} + 1 - \sigma^2 + \varsigma, i = 0 \\ \frac{1}{2(n+\lambda)}, i = 1, \dots, 2n \end{cases} \quad (26)$$

where ς is used to incorporate prior information on the probability density function of the states.

$\chi_k(i)$ can be divided as follows:

$$\chi_k(i) = \begin{bmatrix} \chi_k^{\delta\Re}(i)^T & \chi_k^e(i)^T \end{bmatrix}^T. \quad (27)$$

The quaternion error corresponding to $\chi_k^{\delta\Re}(i)$ is given by

$$\chi_k^{\delta q}(i) = \begin{bmatrix} \delta q_{k,0}(i) & \delta \rho_k(i)^T \end{bmatrix}^T \quad (28)$$

which can be calculated from equation (21).

We denote the quaternion-based sigma points by multiplying the error quaternion by the current attitude quaternion

$$\chi_k^q(i) = \chi_k^{\delta q}(i) \otimes q_k. \quad (29)$$

The sigma points obtained from equation (29) propagate forward through process model (9) and the propagated quaternion error is calculated using following equation:

$$\chi_{k+1|k}^{\delta q}(i) = \chi_{k+1|k}^q(i) \otimes \left[\bar{\chi}_{k+1|k}^q \right]^{-1}. \quad (30)$$

$\bar{\chi}_{k+1|k}^q$ is the average quaternion of the propagating quaternion sigma points; explicit details about $\bar{\chi}_{k+1|k}^q$ can be found in [24, 25].

The predicted GRP sigma points $\chi_{k+1|k}^{\delta\Re}(i)$ corresponding to $\chi_{k+1|k}^{\delta q}(i)$ can be calculated from equation (20).

The propagated sigma points of the state can now be determined as

$$\chi_{k+1|k}(i) = \begin{bmatrix} \chi_{k+1|k}^{\delta\Re}(i)^T & \chi_{k+1|k}^e(i)^T \end{bmatrix}^T. \quad (31)$$

The corresponding state prediction and covariance matrix can be calculated, respectively, as

$$\hat{X}_{k+1|k} = \sum_{i=0}^{2n} W^m(i) \chi_{k+1|k}(i) \quad (32)$$

$$P_{x,k+1|k} = \sum_{i=0}^{2n} W^c(i) \left\{ \chi_{k+1|k}(i) - \hat{X}_{k+1|k} \right\} \times \left\{ \chi_{k+1|k}(i) - \hat{X}_{k+1|k} \right\}^T + Q_k \quad (33)$$

where Q_k denote the process noise covariance matrix at time instant k .

3.2. Measurement update

Similar to equation (24), the new sigma points $\chi_{k+1|k}^*(i)$ are regenerated using $\hat{X}_{k+1|k}$ and $P_{x,k+1|k}$. Similar to equations (27)–(29), the new quaternion-based sigma points $\chi_{k+1|k}^{*q}(i)$ can be obtained, and we define a new set of sigma points as

$$\gamma_{k+1|k}^*(i) = \begin{bmatrix} \chi_{k+1|k}^{*q}(i)^T & \chi_{k+1|k}^{*e}(i)^T \end{bmatrix}^T. \quad (34)$$

The propagated sigma points in (34) are propagated directly through the measurement model (23), the predicted sigma points are $Z_{k+1|k}(i)$.

The predicted mean of measurement, the covariance matrix of measurement and the cross-covariance matrix of the state and measurement are calculated, respectively, as

$$\hat{Y}_{k+1} = \sum_{i=0}^{2n} W^m(i) Z_{k+1|k}(i) \quad (35)$$

$$P_{y,k+1} = \sum_{i=0}^{2n} W^c(i) \left\{ Z_{k+1|k}(i) - \hat{Y}_{k+1} \right\} \times \left\{ Z_{k+1|k}(i) - \hat{Y}_{k+1} \right\}^T + R_k. \quad (36)$$

$$P_{xy,k+1} = \sum_{i=0}^{2n} W^c(i) \left\{ \left(\chi_{k+1|k}^*(i) - \hat{X}_{k+1|k} \right) \times \left(Z_{k+1|k}(i) - \hat{Y}_{k+1} \right)^T \right\}. \quad (37)$$

The innovation vector is given by

$$e_{k+1} = y_{k+1} - \hat{Y}_{k+1}. \quad (38)$$

3.2.1. Estimation of measurement noise covariance matrices. Taking the variance on both side of formula (38) simultaneously we can get

$$E[e_{k+1}e_{k+1}^T] = \left(h(X_{k+1}) + v_{k+1} - \hat{Y}_{k+1} \right) \times \left(h(X_{k+1}) + v_{k+1} - \hat{Y}_{k+1} \right)^T \\ = \left(h(X_{k+1}) - \hat{Y}_{k+1} \right) \times \left(h(X_{k+1}) - \hat{Y}_{k+1} \right)^T + R_{k+1} \quad (39)$$

$$\left(h(X_{k+1}) - \hat{Y}_{k+1} \right) \times \left(h(X_{k+1}) - \hat{Y}_{k+1} \right)^T = P_{y,k+1} - R_k. \quad (40)$$

According to equations (39) and (40), the measurement noise covariance matrix R_{k+1} is given by

$$R_{k+1} = E[e_{k+1}e_{k+1}^T] - P_{y,k+1} + R_k \\ = \frac{1}{k} \sum_{i=1}^k \left(e_{i+1}e_{i+1}^T - P_{y,k+1} + R_i \right) \\ = \frac{1}{k} \left[\sum_{i=1}^{k-1} \left(e_{i+1}e_{i+1}^T - P_{y,k+1} + R_i \right) \right. \\ \left. + \left(e_{k+1}e_{k+1}^T - P_{y,k+1} + R_k \right) \right] \\ = \left(1 - \frac{1}{k} \right) R_k + \frac{1}{k} \left(e_{k+1}e_{k+1}^T - P_{y,k+1} + R_k \right). \quad (41)$$

In order to improve the adaptive ability of equation (41), it is rewritten as

$$R_{k+1} = (1 - \eta_{k+1})R_k + \eta_{k+1} \left(e_{k+1}e_{k+1}^T - P_{y,k+1} + R_k \right) \quad (42)$$

$$\eta_{k+1} = \frac{\eta_k}{\eta_k + c} \quad (43)$$

where $\eta_0 = 1$ and c is called the fading factor, which is usually between 0.9 and 0.999.

In order to improve the reliability of R_k in the adaptive process, sequential filtering is adopted and the upper boundary limit $R_{\max}^{(i)}$ and lower boundary limit $R_{\min}^{(i)}$ are set on each diagonal component of R_k , forcing it to be in a reasonable range all the time. The superscript (i) represents the i th element of the matrix. Equation (42) can be rewritten as

$$R_{k+1}^{(i)} = \begin{cases} (1 - \eta_{k+1})R_k^{(i)} + \eta_{k+1}R_{\min}^{(i)} & p_{k+1}^{(i)} < R_{\min}^{(i)} \\ R_{\max}^{(i)} & p_{k+1}^{(i)} > R_{\max}^{(i)} \\ (1 - \eta_{k+1})R_k^{(i)} + \eta_{k+1}p_{k+1}^{(i)} & \text{others} \end{cases} \quad (44)$$

$$p_{k+1}^{(i)} = e_{k+1}^{(i)} e_{k+1}^{(i)T} - P_{y,k+1}^{(i)} + R_k^{(i)}. \quad (45)$$

3.2.2. Adaptive unscented H-infinite filter. We define the cost function J as

$$J = \frac{\sum_{k=0}^{N-1} \|S_k - \hat{S}_k\|^2}{\|X_0 - \hat{X}_0\|_{P_0^{-1}}^2 + \sum_{k=0}^{N-1} (\|w_k\|_{Q_k^{-1}}^2 + \|v_k\|_{R_k^{-1}}^2)} \quad (46)$$

where X_0 and \hat{X}_0 are the ideal value of the initial system state variables and its estimation results, respectively. $\|A\|_W^2$ is defined as the square of the weighted h_2 norm of A , i.e. $\|A\|_W^2 = A^T W A$. N denotes the filtering time. S_k is the estimation matrix; in this paper, the estimation matrix denotes direct estimation of system state variables. P_0 represents the initial state covariance matrix. w_k denotes the process noise at time instant k .

According to the H-infinite filter theory in [26], the central idea of an H-infinite filter is to ensure that the maximum energy gain from interference signal to estimation error is a minimum, that is to say, the H-infinite norm of the cost function is smallest. Therefore, the influence of disturbance and model uncertainty on the system output is minimized by satisfying the following criteria:

$$\min_{\hat{S}_k} \sup_{X_0, w \in h_2, v \in h_2} J = \gamma^2. \quad (47)$$

By using the statistical linear error propagation method, $P_{y,k+1}$ and $P_{xy,k+1}$ can be approximated by

$$P_{y,k+1} = H_{k+1} P_{x,k+1|k} H_{k+1}^T + R_{k+1} \quad (48)$$

$$P_{xy,k+1} = P_{x,k+1|k} H_{k+1}^T \quad (49)$$

where H_{k+1} is the Jacobian matrices of the nonlinear functions $h(X_{k+1})$.

Based on the extended H-infinite filter in [27], using equations (38), (48) and (49), the updated equations for the state vector and covariance matrix are determined by

$$\hat{X}_{k+1} = \hat{X}_{k+1|k} + P_{xy,k+1} P_{y,k+1}^{-1} e_{k+1} \quad (50)$$

$$P_{x,k+1} = P_{x,k+1|k} - \begin{bmatrix} P_{xy,k+1} & P_{x,k+1|k} \end{bmatrix} R_{e,k+1}^{-1} \times \begin{bmatrix} P_{xy,k+1} & P_{x,k+1|k} \end{bmatrix}^T \quad (51)$$

where

$$R_{e,k+1} = \begin{bmatrix} P_{y,k+1} & P_{xy,k+1}^T \\ P_{xy,k+1} & P_{x,k+1|k} - \gamma^2 I \end{bmatrix}. \quad (52)$$

It can be seen from the above equation that the parameter γ will affect the positiveness of $P_{x,k+1}$. When γ is small, the robustness of the system is strong but the filtering accuracy of the system decreases. When γ is large, the robustness of the system decreases but the filtering accuracy of the system increases. Therefore, an adaptive γ is proposed to ensure the robustness of the system while ensuring accuracy.

By applying the matrix inversion lemma [28] for equation (51), we can get

$$P_{x,k+1}^{-1} = P_{x,k+1|k}^{-1} + P_{x,k+1|k}^{-1} P_{xy,k+1} R_{k+1}^{-1} \left(P_{x,k+1|k}^{-1} P_{xy,k+1} \right)^T - \gamma^{-2} I > \mathbf{0}. \quad (53)$$

By rearranging the above equation, we can get

$$\gamma^2 > \max \left\{ \text{eig} \left(P_{x,k+1|k}^{-1} + P_{x,k+1|k}^{-1} P_{xy,k+1} R_{k+1}^{-1} \times \left(P_{x,k+1|k}^{-1} P_{xy,k+1} \right)^T \right)^{-1} \right\} \quad (54)$$

where $\max \{ \text{eig}(A)^{-1} \}$ represents the maximum eigenvalue of matrix A^{-1} .

Let $\gamma_a = \max \left\{ \text{eig} \left(P_{x,k+1|k}^{-1} + P_{x,k+1|k}^{-1} P_{xy,k+1} R_{k+1}^{-1} \left(P_{x,k+1|k}^{-1} P_{xy,k+1} \right)^T \right)^{-1} \right\}$, then the adaptive γ can be written as

$$\gamma = \begin{cases} \left(1 + k_0 \sqrt{\frac{\text{trace}(P_{y,k+1})}{e_{k+1}^T e_{k+1}}} \right) \gamma_a & \gamma > \gamma_{\min} \\ \gamma_{\min} & \gamma < \gamma_{\min} \end{cases} \quad (55)$$

where k_0 is a correlation coefficient and $k_0 > 0$, which is determined according to the actual situation of the system through the experiment; $\text{trace}(A)$ denotes the trace of the matrix A . γ_{\min} is the lower boundary limit set to ensure the accuracy of alignment and the stability of the system.

Finally, by setting the upper boundary limit γ_{\max} , equation (51) is optimized as

$$\mathbf{P}_{x,k+1} = \begin{cases} \mathbf{P}_{x,k+1|k} - [\mathbf{P}_{xy,k+1} & \mathbf{P}_{x,k+1|k}] \mathbf{R}_{e,k+1}^{-1} \begin{bmatrix} \mathbf{P}_{xy,k+1}^T \\ \mathbf{P}_{x,k+1|k}^T \end{bmatrix} & \gamma < \gamma_{\max} \\ \mathbf{P}_{x,k+1|k} - \mathbf{P}_{xy,k+1} \mathbf{P}_{y,k+1}^{-1} \mathbf{P}_{y,k+1} (\mathbf{P}_{xy,k+1} \mathbf{P}_{y,k+1}^{-1})^T & \gamma > \gamma_{\max} \end{cases} \quad (56)$$

3.3. Attitude update

The updated status vector is expressed as

$$\hat{\mathbf{X}}_{k+1} = [\delta \mathfrak{R}_{k+1}^T \quad \mathbf{X}_{k+1}^e{}^T]^T \quad (57)$$

The quaternion error corresponding to $\delta \mathfrak{R}_{k+1}$ is given by

$$\delta \mathbf{q}_{k+1} = [\delta q_{k+1,0} \quad \delta \boldsymbol{\rho}_{k+1}^T]^T \quad (58)$$

which can be calculated according to equation (24).

The attitude quaternion is updated through

$$\mathbf{q}_{k+1} = \delta \mathbf{q}_{k+1} \otimes \bar{\mathbf{X}}_{k+1|k}^{*q} \quad (59)$$

where $\bar{\mathbf{X}}_{k+1|k}^{*q}$ is the average quaternion of the propagating quaternion sigma points $\mathbf{X}_{k+1|k}^{*q}(i)$.

Resetting $\delta \mathfrak{R}_{k+1}$ to zeros goes to the next filtering cycle.

4. Vehicle-mounted field test

To verify the performance of the proposed AUSQUHE, two vehicle tests were carried out in Changsha. Figure 1 shows the test equipment, which include a self-developed IMU, a dual-antenna GPS receiver, a navigation computer and a self-made LDV. The IMU consists of three ring laser gyroscopes with bias instability of $0.008^\circ \text{h}^{-1}$ and random walk of $0.003^\circ \text{h}^{-1/2}$ and three quartz accelerometers with bias instability of $50 \mu\text{g}$ and random walk of $50 \mu\text{g h}^{-1/2}$. The velocity measurement error of the LDV is 0.1% (1σ) and is calibrated in advance. The data update frequency of the GPS is 10 Hz, and the horizontal position accuracy and altitude accuracy are within 0.1 m. The data output frequency of both the IMU and LDV is 100 Hz. The vehicle remains stationary at the start point for about 13 min before moving and static attitude alignment is performed to obtain an accurate initial attitude. Since the initial conditions are very accurate, the attitude information obtained by SINS/GPS-integrated navigation is used as the reference attitude to evaluate the proposed alignment method. The movement trajectories of the vehicle and the outputs of the LDV are shown in figures 2 and 3, respectively. As can be seen from figure 3, the LDV output of the second vehicle is seriously disturbed by noise.

The following five alignment schemes are designed to evaluate the alignment performance of the proposed scheme:

scheme 1: method proposed in this paper

scheme 2: the OBA method proposed in [9]

scheme 3: the USQUE method proposed in [18]

scheme 4: the AUSQUE method

scheme 5: the alignment method obtained with an H-infinite filter combined with USQUE.

In each test group, the initial value of the attitude quaternion is set as $[1 \ 0 \ 0 \ 0]^T$ for the five schemes. For schemes 1, 3, 4 and 5, the initial covariance matrix of attitude error is set as $\text{diag}([3^\circ \ 3^\circ \ 12^\circ]^T)^2$, and the process noise covariance matrix and initial measurement noise covariance matrix are set as $\text{diag}([10^{-7^\circ} \ 10^{-7^\circ} \ 10^{-7^\circ}]^T)^2$ and $\text{diag}([0.07 \ 0.07 \ 0.07]^T)^2$, respectively. The attitude errors of different schemes in the first vehicle test are shown in figures 4–6.

As can be seen from figures 4–6, the difference in the horizontal angle errors among the five schemes is not significant after 100 s. During the first 100 s of alignment, the convergence speeds of the horizontal angle errors of schemes 1 and 4 are much the same and are the fastest, scheme 3 has the slowest convergence speed and the convergence speeds of schemes 2 and 5 are in the middle, but the convergence speed of scheme 5 is faster than that of scheme 2. Unlike the horizontal angle errors, the heading angle errors of the five schemes are obviously different. In figure 6, the convergence speeds of schemes 1, 4 and 5 are much the same, but schemes 1 and 4 have higher accuracy and stronger robustness than scheme 5, and the accuracy of scheme 1 is slightly higher than that of scheme 4. Scheme 3 has the slowest convergence speed and the worst alignment accuracy. The convergence speed and alignment accuracy of scheme 2 are in the middle.

Compared with schemes 2–4, the influence of disturbance and model uncertainty on the system output is minimized in scheme 1. Additionally, scheme 1 adopts the measurement noise matrix and threshold γ while scheme 5 does not, which makes the system robust without sacrificing too much accuracy. To sum up, the performance of scheme 1 is superior to the other schemes in the first vehicle test.

In order to further test the robustness of the proposed scheme, the threshold of the LDV was adjusted in the second set of vehicle tests, so that the LDV cannot filter the noise signal effectively; the attitude errors of different schemes in the second vehicle test are shown in figures 7–9. It can be seen from figures 7–9 that, compared with other schemes, the performance of scheme 1 is still the best, as the alignment accuracy and the convergence speed of scheme 1 are far superior to those of the other schemes. When the output of LDV is disturbed by noise, scheme 1 still has satisfactory alignment accuracy while the other schemes cannot carry out alignment

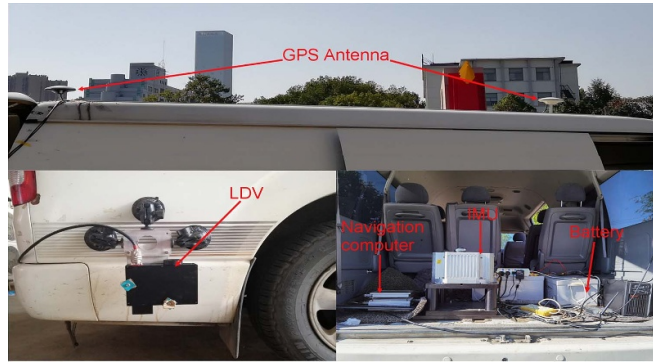


Figure 1. Installation diagram for the experimental system.

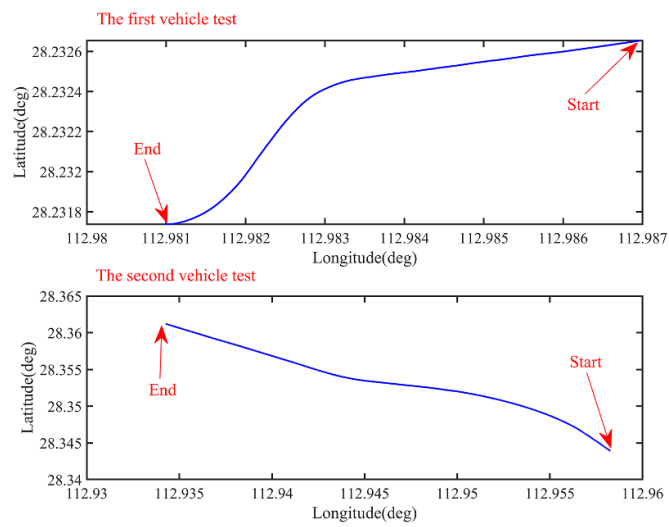


Figure 2. Two trajectories of the vehicle in the field test.

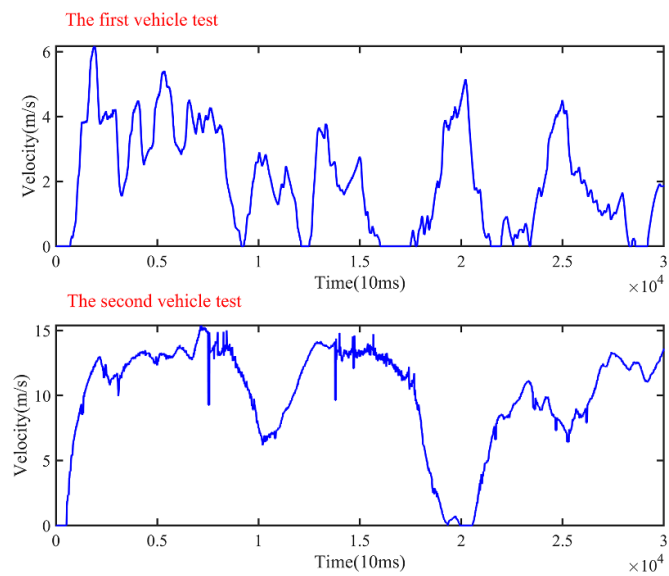


Figure 3. Velocity curves of LDV output.

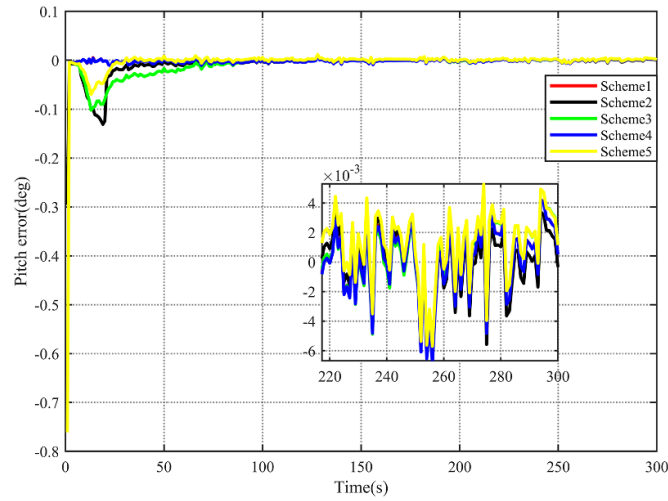


Figure 4. Pitch angle errors by different schemes in the first vehicle test.

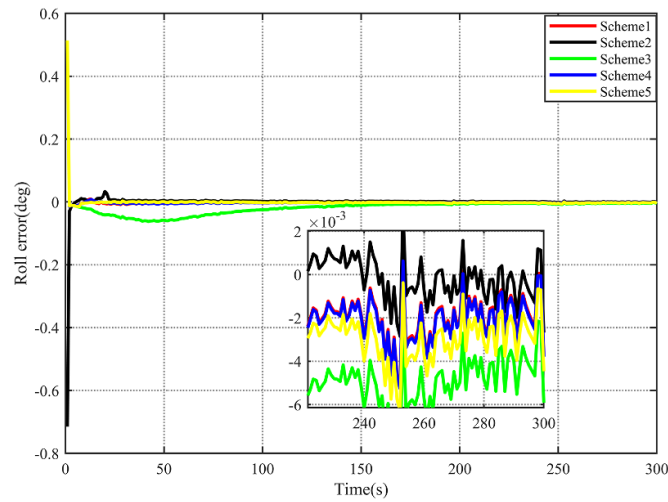


Figure 5. Roll angle errors by different schemes in the first vehicle test.

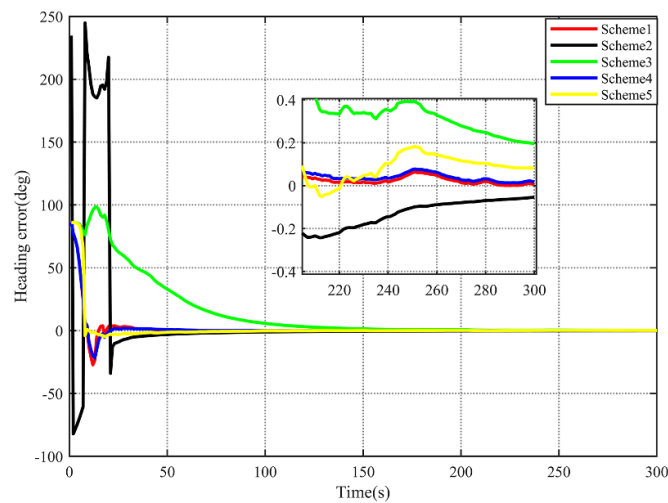


Figure 6. Heading angle errors by different schemes in the first vehicle test.

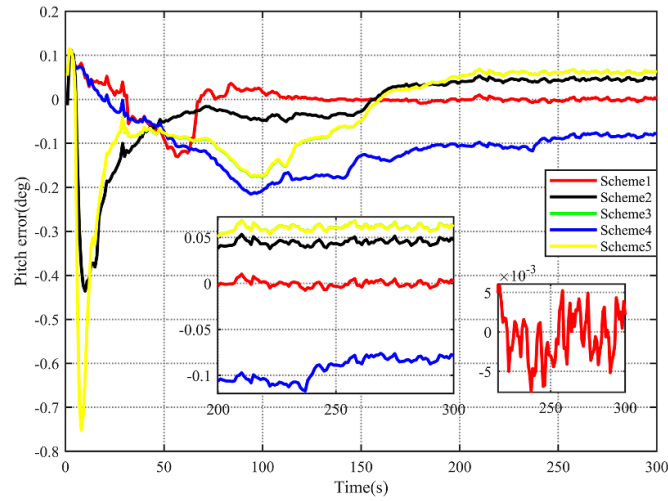


Figure 7. Pitch angle errors by different schemes in the second vehicle test.

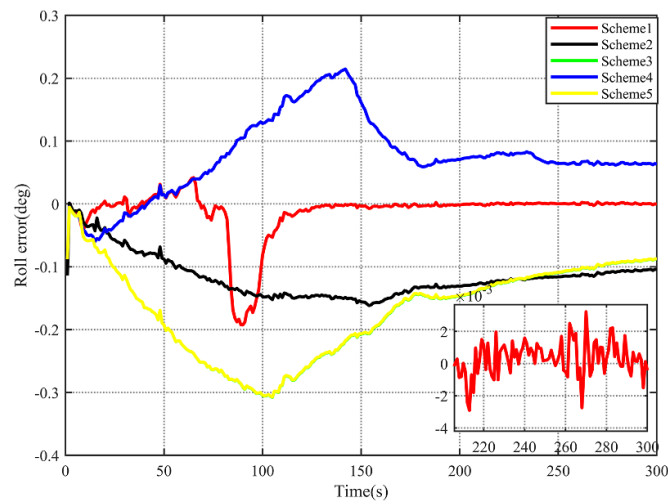


Figure 8. Roll angle errors by different schemes in the second vehicle test.

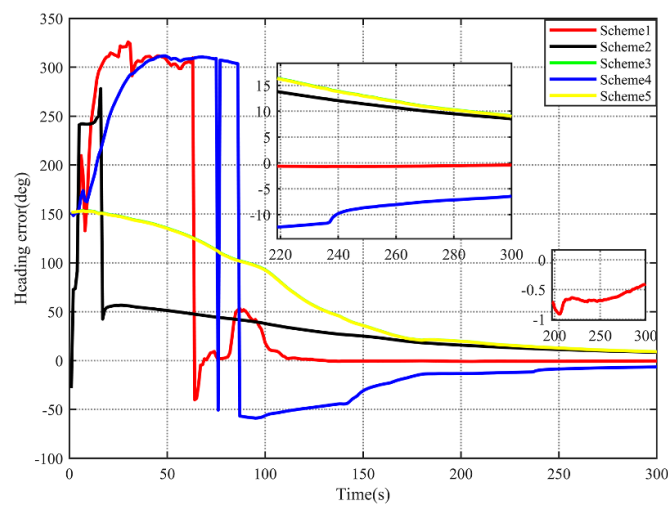


Figure 9. Heading angle errors by different schemes in the second vehicle test.

Table 1. Statistics of the heading angle errors of vehicle in the first vehicle test.

		Time (s)		
		1–90	1–180	181–300
Scheme 1	Mean	4.5305	−0.0629	0.0261
	STD	17.9068	0.0347	0.0168
Scheme 2	Mean	23.8523	−0.6669	−0.1545
	STD	79.8593	0.2515	0.0799
Scheme 3	Mean	43.8600	2.7299	0.3911
	STD	29.0322	1.8951	0.1659
Scheme 4	Mean	4.2385	−0.0176	0.0426
	STD	17.8764	0.0285	0.0186
Scheme 5	Mean	4.9030	−0.0916	0.0903
	STD	22.5246	0.0897	0.0576

Table 2. Statistics of the heading angle errors of vehicle in the second vehicle test.

		Time (s)		
		1–120	121–180	181–300
Scheme 1	Mean	155.2387	−0.2596	−0.6237
	STD	141.2276	0.5144	0.1205
Scheme 2	Mean	65.9164	24.6140	12.4455
	STD	61.5175	3.7126	2.7695
Scheme 3	Mean	120.9258	37.0303	14.5144
	STD	27.0361	11.9686	3.9573
Scheme 4	Mean	178.4269	−32.4598	−10.1751
	STD	156.4519	12.1312	2.6554
Scheme 5	Mean	120.6761	36.9096	14.4593
	STD	27.0265	11.9503	3.9424

at short notice. Compared with the results of the first vehicle test, the results of the second vehicle test show that scheme 1 has the best robustness and alignment accuracy under harsh conditions.

In order to compare the alignment performance of the four schemes more specifically, the mean and standard deviation (STD) are compared. The statistics are shown in tables 1 and 2.

From table 1 we can see that the means of the heading angle errors of schemes 1, 4 and 5 are little different and smaller than those for schemes 2 and 3 between 1 and 90 s, illustrating that the convergence speeds of schemes 1, 4 and 5 are faster than those of schemes 2 and 3. The mean and STD of scheme 1 for 181–300 s are the smallest among the five schemes, which shows that scheme 1 has the best performance at 180–300 s. Table 2 tells us that that when the output of the LDV is disturbed by noise, the mean and STD of scheme 1 at 120–300 s are obviously smaller than those of the other schemes, implying that the advantage of scheme 1 in the second vehicle test is more significant than that in the first vehicle test. Therefore, scheme 1 is more suitable for in-motion alignment than the other schemes.

Considering the requirements for the amount of calculation for the algorithm in practical engineering applications, we compared the time required for computer processing of the alignment process data in two vehicle tests according to

Table 3. Time complexity comparison of different schemes.

Scheme	Time (s)	
	Test 1	Test 2
Scheme 1	19.5758	18.4083
Scheme 2	13.5719	12.6162
Scheme 3	17.2963	16.3573
Scheme 4	17.7083	16.6753
Scheme 5	18.4216	17.4598

different schemes (table 3). As can be seen from table 3, the time complexity of scheme 1 is not much more than that of the other schemes. Compared with the superior performance of scheme 1, the amount of increased computation is acceptable. Therefore, scheme 1 is promising for practical engineering applications.

5. Conclusion

The quality of the initial alignment results will directly affect the subsequent navigational accuracy. A faster robust in-motion initial alignment method, named AUSQUHE, for LDV-aided SINS is proposed in this paper. First, the process model and measurement model for LDV-aided SINS in-motion alignment is derived through skillful attitude matrix decomposition and velocity kinematic equation reconstruction. AUSQUHE is proposed in order to reduce the influence of both approximations in the modeling process, namely the uncertainty noise of the sensors during the motion process and the inaccurate noise parameter setting in the filtering process. The performance of AUSQUHE is much better than that of the other methods in the comparison as it uses H-infinite filter theory and introduces an adaptive noise covariance matrix and adaptive H-infinite filtering threshold. Two vehicle tests were carried out to verify the robustness and accuracy of the proposed in-motion alignment method. The test results show that the performance of the proposed method is better than that of the other compared methods, regardless of whether the LDV signal is disturbed by noise or not. When the LDV signal is disturbed by noise, the advantages of the proposed scheme are more obvious.

Data availability statement

The data that support the findings of this study are available upon reasonable request from the authors.

Acknowledgments

This research was financially supported by the Major Basic Autonomous Research Project of the College of Advanced Interdisciplinary Studies, National University of Defense Technology (ZDJC19-12).

ORCID iD

Jian Zhou  <https://orcid.org/0000-0001-6443-2644>

References

- [1] Wang Q, Gao C, Zhou J, Wei G, Nie X and Long X 2018 Two-dimensional laser Doppler velocimeter and its integrated navigation with a strapdown inertial navigation system *Appl. Opt.* **57** 3334
- [2] Titterton D H, Weston J L and Weston J 2004 *Strapdown Inertial Navigation Technology* 2nd edn (London: The Institution of Electrical Engineers)
- [3] Groves P D 2008 *Principles of GNSS, Inertial, and Multisensor Integrated Navigation Systems* (London: Artech House)
- [4] Lu J, Liang S and Yang Y 2019 Backtracking scheme for single-point self-calibration and rapid in-motion alignment with application to a position and azimuth determining system *Meas. Sci. Technol.* **30** 15102
- [5] Wu Y 2013 Velocity/position integration formula part II: application to strapdown inertial navigation computation *IEEE Trans. Aerosp. Electron. Syst.* **49** 1024–34
- [6] Wu M, Wu Y, Hu X and Hu D 2011 Optimization-based alignment for inertial navigation systems: theory and algorithm *Aerosp. Sci. Technol.* **15** 1–17
- [7] Wu Y and Pan X 2013 Velocity/position integration formula part I: application to in-flight coarse alignment *IEEE Trans. Aerosp. Electron. Syst.* **49** 1006–23
- [8] Zhang Q, Li S, Xu Z and Niu X 2020 Velocity-based optimization-based alignment (VBOBA) of low-end MEMS μ GNSS for low dynamic applications *IEEE Sens. J.* **20** 5527–39
- [9] Zhang Y, Luo L, Fang T, Li N and Wang G 2018 An improved coarse alignment algorithm for odometer-aided SINS based on the optimization design method *Sensors* **18** 195
- [10] Kang L, Ye L and Song K 2014 A fast in-motion alignment algorithm for DVL aided SINS *Math. Probl. Eng.* **2014** 1–12
- [11] Xu X, Xu D, Zhang T and Zhao H 2019 In-motion coarse alignment method for SINS/GPS using position loci *IEEE Sens. J.* **19** 3930–8
- [12] Chang L, Li J and Li K 2016 Optimization-based alignment for strapdown inertial navigation system: comparison and extension *IEEE Trans. Aerosp. Electron. Syst.* **52** 1697–713
- [13] Huang Y, Zhang Y and Wang X 2017 Kalman-filtering-based in-motion coarse alignment for odometer-aided SINS *IEEE Trans. Instrum. Meas.* **66** 3364–77
- [14] Luo L, Huang Y, Zhang Z and Zhang Y 2021 A new Kalman filter-based in-motion initial alignment method for DVL-aided low-cost SINS *IEEE Trans. Veh. Technol.* **70** 331–43
- [15] Luo L, Huang Y, Zhang Z and Zhang Y 2021 A position loci-based in-motion initial alignment method for low-cost attitude and heading reference system *IEEE Trans. Instrum. Meas.* **70** 1–18
- [16] Huang Y, Zhang Y and Chang L 2018 A new fast in-motion coarse alignment method for GPS-aided low-cost SINS *IEEE/ASME Trans. Mechatronics* **23** 1303–13
- [17] Chang L, Li Y and Xue B 2017 Initial alignment for a Doppler velocity log-aided strapdown inertial navigation system with limited information *IEEE/ASME Trans. Mechatronics* **22** 329–38
- [18] Chang L, He H and Qin F 2017 In-motion initial alignment for odometer-aided strapdown inertial navigation system based on attitude estimation *IEEE Sens. J.* **17** 766–73
- [19] Jian Z and Xingwu L 2010 Research on laser Doppler velocimeter for vehicle self-contained inertial navigation system *Opt. Laser Technol.* **42** 477–83
- [20] Nie X and Zhou J 2020 Pitch independent vehicle-based laser Doppler velocimeter *Opt. Lasers Eng.* **131** 106072
- [21] Zhou J, Nie X and Lin J 2014 A novel laser Doppler velocimeter and its integrated navigation system with strapdown inertial navigation *Opt. Laser Technol.* **64** 319–23
- [22] Wang Q, Nie X, Gao C, Zhou J, Wei G and Long X 2018 Calibration of a three-dimensional laser Doppler velocimeter in a land integrated navigation system *Appl. Opt.* **57** 8566–72
- [23] Huang R, Wang Q, Nie X and Zhou J 2020 One-dimensional reference-beam LDV for accurate altitude estimation in a land vehicle *Appl. Opt.* **59** 10667–72
- [24] Markley F L, Cheng Y, Crassidis J L and Oshman Y 2007 Averaging quaternions *J. Guid. Control. Dyn.* **30** 1193–7
- [25] Chang L, Hu B and Chang G 2014 Modified unscented quaternion estimator based on quaternion averaging *J. Guid. Control. Dyn.* **37** 305–8
- [26] Wang J, Chen X and Yang P 2021 Adaptive H-infinite kalman filter based on multiple fading factors and its application in unmanned underwater vehicle *ISA Trans.* **108** 295–304
- [27] Zhao J, Netto M and Mili L 2017 A robust iterated extended Kalman filter for power system dynamic state estimation *IEEE Trans. Power Syst.* **32** 3205–16
- [28] Zhou K, Doyle J C and Glover K 2002 Robust and optimal control *35th IEEE Conf. Decision and Control IEEE Conf. Decis. Control (Kobe, Japan)* (<https://doi.org/10.1109/CDC.1996.572756>)